

Design and Optimization of Gadolinium Based Contrast Agents for Magnetic Resonance Imaging

G. A. Pereira, C. F. G. C. Geraldes*

Department of Biochemistry, Faculty of Science and Technology, and Center of Neurosciences and Cell Biology, University of Coimbra, 3001-401 Coimbra, Portugal
geraldes@bioq.uc.pt

Keywords: Gadolinium complexes; contrast agents; magnetic resonance imaging; NMR.

Abstract: *The role of Gd³⁺ chelates as contrast agents in Magnetic Resonance Imaging is discussed. The theory describing the different contributions to paramagnetic relaxation relevant to the understanding of the molecular parameters determining the relaxivity of those Gd³⁺ chelates, is presented. The experimental techniques used to obtain those parameters are also described. Then, the various approaches taken to optimize those parameters, leading to maximum relaxivity (efficiency) of the contrast agents, are also illustrated with relevant examples taken from the literature. The various types of Gd³⁺-based agents, besides non-specific and hepatobiliary agents, are also discussed, namely blood pool, targeting, responsive and paramagnetic chemical shift saturation transfer (PARACEST) agents. Finally, a perspective is presented of some of the challenges lying ahead in the optimization of MRI contrast agents to be useful in Molecular Imaging.*

1. Magnetic Resonance Imaging

Magnetic Resonance Imaging (MRI) is based on the principles of Nuclear Magnetic Resonance (NMR), a spectroscopic technique used by scientists to obtain microscopic chemical and physical information about molecules. The magnetic resonance phenomenon was described first by Felix Bloch and Edward Purcell in 1946. Between 1950 and 1970, the NMR technique was developed to analyze the chemical and physical properties in organic molecules.

Raymond Damadian in 1971 showed that the nuclear magnetic relaxation times, T_1 and T_2 , of tissues and tumors are different, motivating scientists to consider magnetic resonance for the detection of diseases.¹ Magnetic resonance imaging was first demonstrated in 1973 by Paul Lauterbur and Mansfield.^{2a,b} Nowadays, Magnetic Resonance Imaging is considered one of the most powerful diagnostic techniques developed. The

main advantages in the use of MRI as imaging technique (comparing with others, such as PET and CT) are that (i) no ionization radiation is used, avoiding to expose the patient being scanned to the health risk from radiation, (ii) in case the tissue is diseased, the values of T_1 and T_2 change, consequently changing the images, (iii) it is possible to get a better spatial resolution, which in the case of MRI is 0.2-0.3 mm, while the PET technique has a spatial resolution of about 3 mm, and (iv) the image can be created in any wished direction in the human body. The limitations of the MRI images are that (i) the bones are not visualized, (ii) it can not be used by people with pacemakers or other implanted magnetizable metal parts and (iii) the price of a MRI scanner is still more expensive than the price for CT. A good account of the evolution of the MRI technique, since the discovery to the present, has been published.³

The NMR signal of body water protons is used to generate the MRI images. This was

chosen due to the high NMR sensitivity and the high natural abundance of protons and also because ~ 70% in weight of the human body is constituted by water. To create an MRI image constituted by different voxels (volume picture elements) of the subject, magnetic field gradients are applied along three perpendicular directions. Although it is relatively common to apply gradients in the principal axes of a patient (so that the patient is imaged in x, y, and z from head to toe), MRI allows completely flexible orientations for images. All spatial encoding is obtained by applying magnetic field gradients which encode the position within the phase of the signal. In one dimension, a linear relationship of phase with respect to position can be obtained by collecting data in the presence of a magnetic field gradient. In three dimensions (3D), a plane can be defined by "slice selection", in which an RF pulse of defined bandwidth is applied in the presence of a magnetic field gradient in order to reduce spatial encoding to two dimensions (2D). Spatial encoding can then be applied in 2D after slice selection, or in 3D without slice selection. Spatially-encoded phases are recorded in a 2D or 3D matrix; this data represents the spatial frequencies of the image object. Images can be created from the matrix using the discrete Fourier transform (DFT). Typical medical resolution is about 1mm^3 , while research models can exceed $1\mu\text{m}^3$. The contrast in the MRI image is determined by the difference in signal intensities in the various voxels.^{3,4}

MRI images can be obtained by using numerous pulse sequences, although the most common is a spin-echo sequence (Fig. 1). It uses 90° radio frequency pulses to excite the magnetization and one or more 180° pulses to refocus the spins to generate signal echoes named spin echoes (SE). Three types of gradients are applied, for slice selection (GS), phase encoding (GP) and frequency encoding (GF). An advantage of using a spin-echo sequence is that it introduces T_2 dependence to the signal intensity, because some tissues and pathologies have similar T_1 values but different T_2 values and it is advantageous to have an imaging sequence which produces images with T_2 dependence. The pulse sequence timing can be adjusted to give T_1 -weighted, proton or spin density, and T_2 -weighted images. In T_1 -weighted images, the tissues with shorter T_1 values give a brighter image and for those with longer T_1 darker images are obtained. The two variables of interest in spin echo sequences are the repetition time (TR) and the echo time (TE), in which TR is defined as the time between repetitions of the sequence and TE is the time between the 90° pulse and the maximum amplitude in the echo, respectively. The signal intensity (SI) is given by Eq. 1, where k is a proportionality constant dependent on flow, perfusion and diffusion, and ρ is the density of spins in the sample.⁴

$$SI = k \rho (1 - e^{-TR/T_1}) e^{-TE/T_2} \quad (1)$$

2. MRI Contrast Agents

Paramagnetic chelates containing a lanthanide ion, namely gadolinium (III) are generally used as contrast agents (CAs). The Gd^{3+} ion has physical properties which are suitable for reducing the longitudinal (T_1) and transverse (T_2) proton relaxation times. It possesses seven unpaired electrons (highest

spin density) and a symmetrical 8S ground state, resulting in a slower electronic relaxation rate. Since the Gd^{3+} ion undergoes a rapid hydrolysis at physiological pH, producing insoluble $Gd(OH)_3$ and accumulates in bones and liver, a high thermodynamic and kinetic stability of the complexes used as MRI CAs are required, and these properties are fundamental for their use *in vivo*.

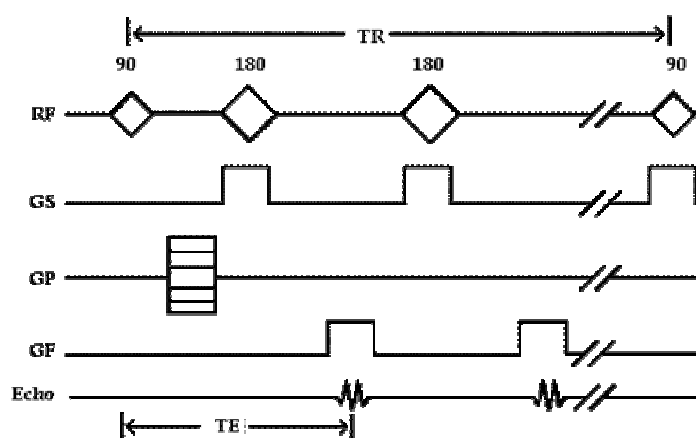


Figure 1. Spin-echo pulse sequence used in MRI.

The efficiency of the MRI CAs is measured in terms of the *relaxivity* (r) that indicates their ability to decrease the relaxation times of the water protons per unit (mM) concentration of the CA. The contrast enhancement is obtained when one tissue has either higher affinity for the CAs or higher vascularity than another one. Diseased tissues, such as tumors, are metabolically different compared with healthy

tissues and they have much higher uptake of the contrast agents, resulting in a higher contrast in MRI images.

Chelates containing polyaminocarboxilates as Gd^{3+} ligands are the most important class of contrast agents commercially available (Fig. 2) which are intravenously injected.⁵ In 1988, $[Gd(DTPA)(H_2O)]^{2-}$ (Magnevist[®]) was the first

contrast agent to be approved for *in vivo* use, followed by $[\text{Gd}(\text{DOTA})]^-$ (Dotarem[®]).

Currently, Gd^{3+} complexes of DTPA and DOTA derivatives are also used as MRI CA's, such as $[\text{Gd}(\text{DTPA-BMA})(\text{H}_2\text{O})]$ and

$[\text{Gd}(\text{HPDO3A})(\text{H}_2\text{O})]$. These CAs have the advantage of having no charge, and thus perturbing to a lower extent the osmolarity of blood.

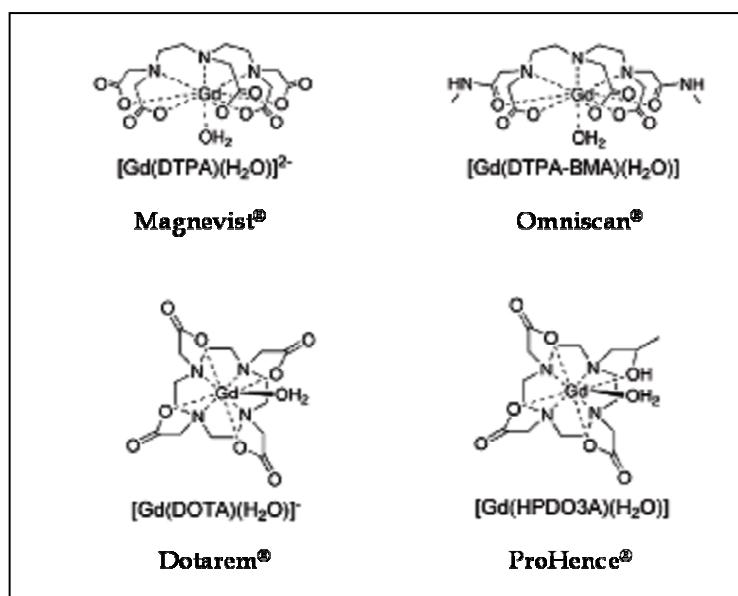


Figure 2. Structures of some Gd^{3+} MRI contrast agents used clinically.⁵

3. Relaxivity

The efficiency of MRI CAs is measured by the relaxivity parameter (r_1). Relaxivity is defined as the ability of magnetic compounds to increase the relaxation rates of the surrounding water proton spins, which are used to improve the contrast of the image and to study tissue specific areas where the contrast agent better diffuses. Relaxivity is expressed in s^{-1} per mM of Gd^{3+} and it

depends on the molecular structure and dynamics of the complex. The paramagnetic relaxation process is described on the basis of a model considering two distinct contributions: 'inner sphere', related to the exchange between the bound water molecules and bulk water, and 'outer sphere', resulting from water molecules diffusing near the paramagnetic centre during their translational diffusion.^{5,6} Often, a third paramagnetic contribution to the relaxivity is taken into account, called 'second-

sphere contribution', that is due to the presence of mobile protons or water molecules in the second coordination sphere of the metal⁷ (Fig. 3).

If the second sphere contribution is not considered, the relaxivity (r_i) can be defined as in Eq. 2, where $T_{i,obs}$ is the observed

longitudinal ($i = 1$) or transverse ($i = 2$) NMR relaxation times, $T_{i,d}$, $T_{i,p}^{is}$ and $T_{i,p}^{os}$ are, respectively, the diamagnetic, the inner- and outer-sphere paramagnetic contributions to the observed relaxation time, and $[Gd^{3+}]$ is the millimolar concentration of the Gd^{3+} complex.

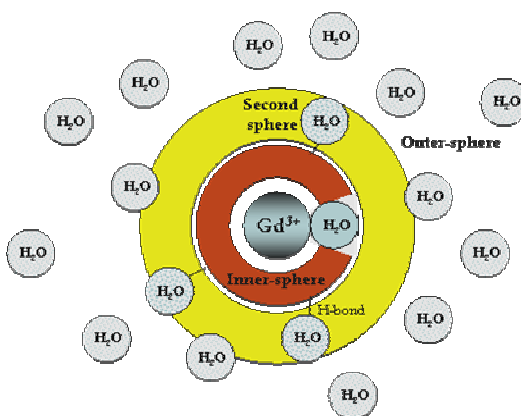


Figure 3. Schematic representation of the three types of water molecules surrounding the metal complex.

$$\frac{1}{T_{i,obs}} = \frac{1}{T_{i,p}^{is}} + \frac{1}{T_{i,p}^{os}} + \frac{1}{T_{i,d}} = r_i [Gd^{3+}] + \frac{1}{T_{i,d}} \quad i = 1,2 \quad (2)$$

3.1. Inner-Sphere Relaxation

The inner-sphere relaxation theory of a paramagnetic centre was developed by Solomon-Bloembergen-Morgan (SBM).⁸⁻¹⁰ The

parameters involved in this inner-sphere mechanism are (i) the number of water molecules directly coordinated to the paramagnetic centre (q), (ii) the molar concentration of the paramagnetic complex

(C), (iii) the mean residence lifetime of the coordinated water protons (τ_M) and (iv) their longitudinal and transverse proton relaxation times (T_{1M} and T_{2M}). This inner-sphere

contribution to the overall relaxation rates is described in Eqs. 3 and 4, where $\Delta\omega_M$ is the chemical shift difference between the free and the bound water molecules.

$$\frac{1}{T_1^{is}} = R_1^{is} = \frac{q[C]}{55.5(T_{1M} + \tau_M)} \quad (3)$$

$$\frac{1}{T_{2,p}^{is}} = R_2^{is} = \frac{q[C]}{55.5\tau_M} \left[\frac{T_{2M}^{-1}(\tau_M^{-1} + T_{2M}^{-1}) + \Delta\omega_M^2}{(\tau_M^{-1} + T_{2M}^{-1})^2 + \Delta\omega_M^2} \right] \quad (4)$$

The inner-sphere contribution becomes important and is transferred to the bulk water when $T_{1M} \gg \tau_M$ where the system is in the 'fast exchange' regime. In the opposite case ($T_{1M} \ll \tau_M$), when the coordinated water molecule is in the 'slow exchange' regime, the water exchange rate becomes the limiting factor of the relaxivity. The relaxation rate of the metal ion coordinated water molecules, ($1/T_{1M}$) is given by the contribution from two mechanisms of electron-nuclear magnetic interaction which

are the dipole-dipole ($1/T_i^{dip}$) mechanism, arising from random fluctuations of the through-space interaction of the nuclear dipole with the unpaired electron dipole, and the scalar ($1/T_i^{SC}$) mechanism, resulting from a through-bond delocalization of the unpaired spin density on the nucleus. Eqs. 5 to 11⁸⁻¹⁰ describe those mechanisms within the SBM approximation:

$$\frac{1}{T_{iM}} = \frac{1}{T_i^{dip}} + \frac{1}{T_i^{SC}} \quad (i = 1, 2) \quad (5)$$

$$\frac{1}{T_1^{dip}} = R_1^{dip} = \frac{2}{15} \cdot \frac{\gamma_I^2 g^2 \mu_B^2 S(S+1)}{r_{GdH}^6} \left(\frac{\mu_o}{4\pi} \right)^2 \left[\frac{3\tau_{e1}}{1 + \omega_I^2 \tau_{e1}^2} + \frac{7\tau_{e2}}{1 + \omega_S^2 \tau_{e2}^2} \right] \quad (6)$$

$$\frac{1}{T_1^{SC}} = R_1^{SC} = \frac{2}{3} S(S+1) \left(\frac{A}{\hbar} \right)^2 \left[\frac{\tau_{e2}}{1 + \omega_S^2 \tau_{e2}^2} \right] \quad (7)$$

$$\frac{1}{T_2^{dip}} = R_2^{dip} = \frac{1}{15} \cdot \frac{\gamma_I^2 g^2 \mu_B^2 S(S+1)}{r_{GdH}^6} \left(\frac{\mu_0}{4\pi} \right)^2 \left[\frac{3\tau_{c1}}{1 + \omega_I^2 \tau_{c1}^2} + \frac{13\tau_{c2}}{1 + \omega_S^2 \tau_{c2}^2} + 4\tau_{c1} \right] \quad (8)$$

$$\frac{1}{T_2^{SC}} = R_2^{SC} = \frac{1}{3} S(S+1) \cdot \left(\frac{A}{\hbar} \right)^2 \left[\frac{\tau_{e2}}{1 + \omega_S^2 \tau_{e2}^2} + \tau_{e1} \right] \quad (9)$$

$$\frac{1}{\tau_{ci}} = \frac{1}{\tau_M} + \frac{1}{\tau_R} + \frac{1}{T_{ie}} \quad (i=1,2) \quad (10)$$

$$\frac{1}{\tau_{ei}} = \frac{1}{\tau_M} + \frac{1}{T_{ie}} \quad (i=1,2) \quad (11)$$

Here, S is the electron spin quantum number, γ is the nuclear gyromagnetic ratio, g is the electron g -factor, μ_B is the Bohr magneton, r_{GdH} is the distance between Gd^{3+} and the water proton, μ_0 is the magnetic permeability of a vacuum, A/\hbar is the hyperfine coupling constant between the metal electrons and the water protons, ω and ω_S are the nuclear and electron Larmor frequencies, respectively ($\omega_{i,S} = \gamma_{i,S} \cdot B$, where B is the magnetic field). Since ω_S is much larger than ω , the terms $|\omega \pm \omega_S|$ can be approximated by ω_S . The correlation times τ_{ci} and τ_{ei} defined by Eqs. 10 and 11, describe the time evolution of the various phenomena influencing the nuclei of interest, where τ_R is the rotational correlation time of the molecule or complex and T_{1e} and

T_{2e} are, respectively, the longitudinal and transverse electron spin relaxation times. Eqs. 6 and 8 show that in the fast motion limit (for small τ_c), R_1^{dip} and R_2^{dip} are almost equal, while far from this limit (for long τ_c) R_1^{dip} decreases with τ_c and R_2^{dip} is constantly increasing due to the presence of the frequency independent term $4\tau_c$. With respect to the contact contribution, SC, due to its nature, the correlation time modulating this contribution is not affected by τ_R (Eqs. 7 and 9) and since $\omega_S^2 \tau_e^2$ is extremely large, for Gd^{3+} complexes, R_1^{SC} is usually negligible, while for R_2 , the contact contribution (R_2^{SC}) is often the

dominant mechanism, mainly for nuclei near the metal ion.¹¹

At high magnetic fields, especially if τ_R is much larger than T_{ie} , the Curie or susceptibility

mechanism is another dipolar effect that must be considered (Eqs. 12 and 13) and it is defined as:¹²

$$\frac{1}{T_{1,\chi}} = \frac{6}{5} \left(\frac{\mu_o}{4\pi} \right)^2 \cdot \frac{\gamma_I^2 g^4 \mu_B^4 S^2 (S+1)^2 B_o^2}{(3kT)^2 r_{GdH}^6} \cdot \left(\frac{\tau_R}{1 + \omega_I^2 \tau_R^2} \right) \quad (12)$$

$$\frac{1}{T_{2,\chi}} = \frac{1}{5} \left(\frac{\mu_o}{4\pi} \right)^2 \cdot \frac{\gamma_I^2 g^4 \mu_B^4 S^2 (S+1)^2 B_o^2}{(3kT)^2 r_{GdH}^6} \cdot \left(4\tau_R + \frac{3\tau_R}{1 + \omega_I^2 \tau_R^2} \right) \quad (13)$$

where B_o is the magnetic field strength, T is the absolute temperature, k is the Boltzmann constant, r_{GdH} is the distance between the nuclear spin and the Ln^{3+} ion. These equations can be simplified by using the effective magnetic moment of the Ln^{3+} ion, $\mu_{\text{eff}} = g\sqrt{S(S+1)}$. The Curie mechanism describes the dipolar interaction between the nuclear spins and the magnetic moment generated by the thermally averaged excess of electron population in the electronic spins levels. The contribution of this mechanism to

the total longitudinal relaxation usually is only relevant for slowly rotating macromolecules (long τ_R).

Finally, the electronic relaxation rates ($1/T_{ie}$) in Gd^{3+} complexes are usually interpreted in terms of a modulation of the zero field splitting (ZFS).^{13,14} A transient ZFS of the spin levels is induced by collisions between solvent molecules and the metal complexes, allowing the coupling of rotation with spin transitions (Eqs. 14 and 15):

$$\left(\frac{1}{T_{ie}} \right)^{\text{ZFS}} = \frac{\Delta^2}{25} \tau_V [4S(S+1) - 3] \left(\frac{1}{1 + \omega_S^2 \tau_V^2} + \frac{4}{1 + 4\omega_S^2 \tau_V^2} \right) \quad (14)$$

$$\left(\frac{1}{T_{2e}} \right)^{\text{ZFS}} = \frac{\Delta^2}{50} \tau_V [4S(S+1) - 3] \left(\frac{5}{1 + \omega_S^2 \tau_V^2} + \frac{2}{1 + \omega_S^2 \tau_V^2} + 3 \right) \quad (15)$$

where τ_V is the correlation time for the distortion of the metal coordination cage and Δ^2 is the mean squared fluctuation of the ZFS interaction.

At low magnetic field ($B_0 < 0.1$ T), the relaxivity of the Gd^{3+} complexes depends mainly on the electronic relaxation (Eq. 16).

$$1/T_{1e}, 1/T_{2e} \gg 1/\tau_R; T_{1e} \approx \tau_{c1}; T_{2e} \approx \tau_{c2} \quad (16)$$

$$1/T_{1e}, 1/T_{2e} \ll 1/\tau_R; \tau_R \approx \tau_{c1} \approx \tau_{c2} \quad (17)$$

This confirms that the major contribution to the observed EPR linewidths is due to electronic relaxation. However, the use of a more recent description of electron spin relaxation needs EPR measurements over a very wide range of temperature and magnetic fields.¹⁶

3.2. Outer-Sphere Relaxation

The outer-sphere contribution is responsible for about 50% of the total relaxivity

At high magnetic field ($B_0 > 1.5$ T) the electronic relaxation rate decreases and becomes slower than the rotational rate of the complex (Eq. 17).

A temperature and magnetic field dependent EPR study¹⁵ has demonstrated that $1/T_{1e}$ of various Gd^{3+} complexes is described, to a good approximation, by these equations.

of small-sized Gd^{3+} complexes. In case of macromolecular systems, the outer sphere contribution is less important.

This contribution to the relaxation is attributed to the modulation of the dipolar interaction by the diffusion of water molecules from the bulk solution close to the metal center.

The outer-sphere relaxation is usually described (Eqs. 18 to 20) using the Freed equations^{17,18} which take into account the electronic relaxation and diffusion:

$$\frac{1}{T_1^{os}} = R_1^{os} = \left(\frac{32\pi}{405}\right) \left(\frac{\mu_o}{4\pi}\right)^2 \cdot \gamma_I^2 \gamma_S^2 \hbar^2 S(S+1) \cdot \frac{N_A}{a_{GdH} \cdot D_{GdH}} \cdot [3J(\omega_I; T_{1e}) + 7J(\omega_S; T_{2e})] \quad (18)$$

$$J(\omega_i; T_{je}) = \text{Re} \left[\frac{1 + \frac{1}{4} \left(i\omega_i \tau_{GdH} + \frac{\tau_{GdH}}{T_{je}} \right)^{\frac{1}{2}}}{1 + \left(i\omega_i \tau_{GdH} + \frac{\tau_{GdH}}{T_{je}} \right)^{\frac{1}{2}} + \frac{4}{9} \left(i\omega_i \tau_{GdH} + \frac{\tau_{GdH}}{T_{je}} \right) + \frac{1}{9} \left(i\omega_i \tau_{GdH} + \frac{\tau_{GdH}}{T_{je}} \right)^{\frac{3}{2}}} \right] \quad (19)$$

$$j = 1, 2 ; i = l, S$$

$$\tau_{GdH} = \frac{a_{GdH}^2}{D_{GdH}} \quad (20)$$

where, T_{je} are the electronic relaxation times, $J(\omega; T_{je})$ is a non-Lorentzian spectral density function, N_A is the Avogadro's number, γ_S is electron gyromagnetic ratio, a_{GdH} is of the closest approach of the solvent protons and the paramagnetic center, D_{GdH} is the sum of the diffusion coefficients of the water proton and of the Gd^{3+} complex and τ_{GdH} is the diffusion correlation time. The symbols not mentioned here maintain the meaning given before. Complexes with similar sizes and shapes have similar diffusion coefficients and the outer-sphere contribution to the relaxivity is also similar in these cases.

It is important to consider that in the outer-sphere relaxation the 'second-sphere' water molecules contribution to the relaxation enhancement is valid, as was mentioned before. These water molecules should be considered as bound via hydrogen bonds to the functional group in the ligand molecule. As the second-sphere contribution is difficult to

evaluate, because the number of second-sphere water molecules and their exchange rates are unknown, usually the second sphere effect is included in the outer sphere contribution. However the unexpected high relaxivity values for some Gd^{3+} complexes, such as $[Gd(DOTP)]^{5-}$, where there are no water molecules in the inner-sphere, could only be explained by considering a very strong second-sphere contribution.¹⁹ For this reason, the inclusion of a second sphere theory⁷ is needed to adjust relaxivity data from Gd^{3+} complexes which present functional groups able to interact strongly with water molecules.

4. Parameters Governing the Paramagnetic Relaxation

The search for more effective contrast agents involves the optimization of various parameters governing the relaxivity. Since the relation between the molecular structure and

electronic relaxation is not well known, this task is focused on the optimization of three parameters, which are the number of water molecules coordinated to the metal ion (q), the exchange lifetime (τ_M) and the reorientational correlation time (τ_R).

Figure 4 represents the inner sphere proton relaxivity (r_1) calculated at two magnetic fields as a function of τ_M and τ_R for some electronic relaxation time values, $q = 1$ and $r = 3.1 \text{ \AA}$. The simulated curves show that the optimal relaxivities can be obtained by slowing down the rotation of the complex and optimizing the exchange lifetime (for the later, either a too long or too short exchange lifetime has a negative influence in the relaxivity). Also, the optimal relaxivity reached decreases with increasing magnetic field strength. When one parameter begins to be optimized the other parameters become more critical. T_{1e} is getting longer as the magnetic field strength increases and at 0.5 T, T_{1e} may be a limiting factor, but at 1.5 T it may reach a point where it does not influence r_1 .

4.1. Number of Coordinated Water Molecules (q)

One structural parameter that influences the inner sphere relaxivity is the number of coordinated water molecules (or hydration number) q .

According to Eq. 3, a higher number of coordinated water provides a clear advantage in terms of efficiency. However there is a limit

to increase the q values, because this would affect the overall thermodynamic and kinetic stabilities of the complex.

Currently, all the commercial contrast agents have only one inner sphere water molecule. Some stable Gd^{3+} complexes containing two inner sphere water molecules have been studied, such as paramagnetic complexes with HOPO²⁰ and PCP2A²¹ as ligands (Fig. 5).

An alternative approach which can be used to increase the paramagnetic relaxation is by increasing the number of water molecules in the second-sphere of coordination by introducing functional groups on the ligand that are capable of forming hydrogen bonds with bulk water molecules.

4.2. Exchange Lifetime (τ_M)

This parameter modulates the chemical exchange from the inner- sphere of the metal to the bulk (Eq. 3) and contributes to the overall correlation time (τ_c) that governs the dipole-dipole interaction between the electron and the nuclear spin (Eqs. 6, 8 and 10).

The proton exchange from the coordinated water molecules to the bulk may occur (i) at pH near neutrality by exchange of the water molecule itself or (ii) independently of the exchange of the entire water molecule on which they reside, by proton exchange at low or high pH.⁵

The water exchange rates of Gd^{3+} complexes used in the MRI technique are

about three orders of magnitude lower than that of the aqua ion $[\text{Gd}(\text{H}_2\text{O})_8]^{3+}$.^{5,22,23} Table 1

shows the water exchange rates ($k_{\text{ex}} = 1/\tau_M$) of various Gd^{3+} complexes.

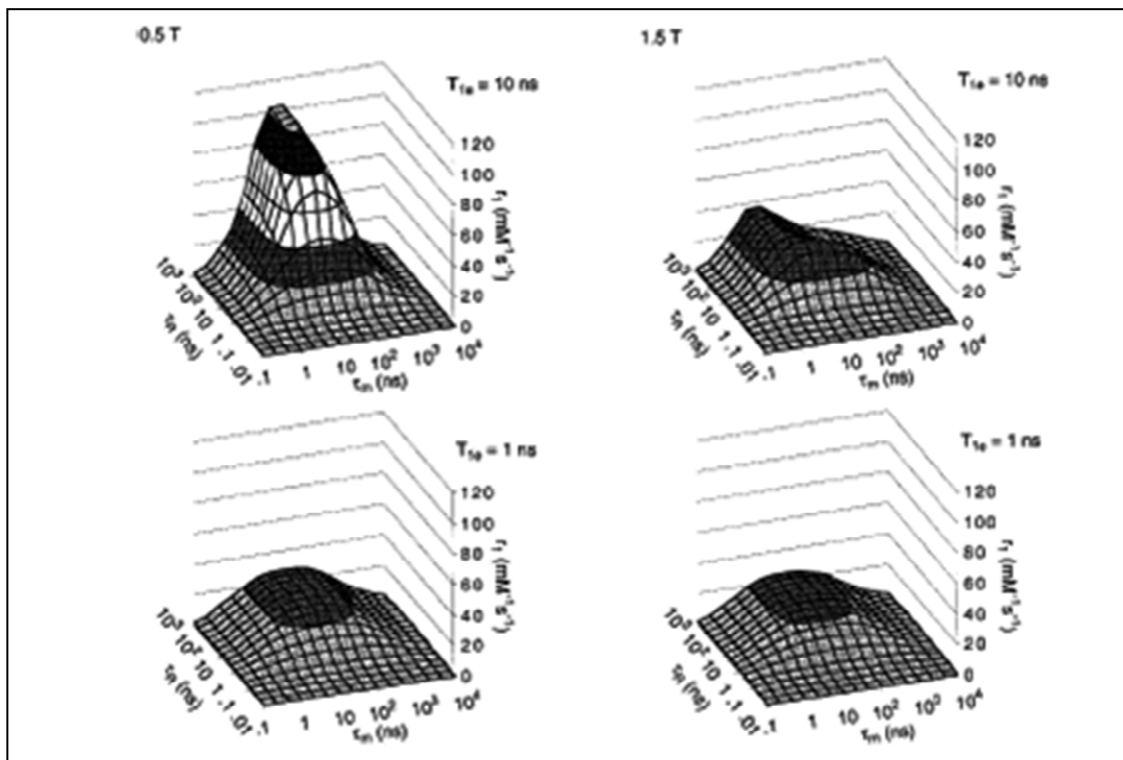


Figure 4. Inner-sphere proton relaxivity as a function of τ_M and τ_R for various values of T_{1e} , $q=1$ and $r = 3.1\text{\AA}$ at 0.5T (~21MHz) and 1.5T (~64MHz).⁵

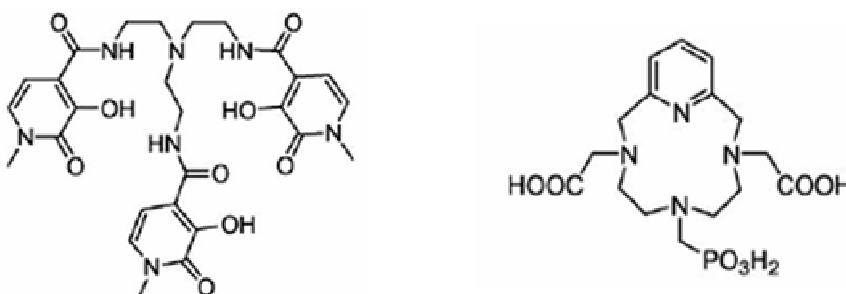


Figure 5. Schematic representation of HOPO (left) and PCP2A ligands^{20,21} containing two water molecules in the inner coordination sphere.

Table 1. Water exchange rates for various Gd³⁺ complexes at 298 K.

Ligand	q	k _{ex} (10 ⁶ s ⁻¹)	Ref.
H ₂ O	8	804	24
DOTA	1	4.10	22
DOTAM	1	0.05	25
DTPA	1	3.30	22
DTPA-P	1	16	26
DTPA-BMA	1	0.43	27
DTPA-EOB	1	3.60	28
DTPA-BGLUCA	1	0.38	29
TRITA	1	270	30
EPTPA	1	330	31

The water exchange lifetime should be short enough to allow efficient transfer of the inner sphere relaxivity to the bulk water, but not so short that it shortens the correlation times for the dipole-dipole interactions (Eq. 10). The ideal water exchange lifetime is found as:

$$\frac{1}{T_{1M}} < \frac{1}{\tau_M} < \frac{1}{\tau_R}, \frac{1}{\tau_S} \quad (21)$$

which corresponds to $k_{ex} \approx 10^8 \text{ s}^{-1}$ (see Table 1). The exchange lifetime of a complex can be influenced by its binding to macromolecules, such as proteins, due to the possibility of hydrogen bonding interactions or to steric blocking of the water exchange pathway.

The optimization of τ_M is a determinant factor to obtain more efficient CA's. Recent studies showed that the water exchange lifetime can be optimized by increasing the crowding near the paramagnetic ion in DTPA and DOTA-like Gd³⁺ complexes. This can be

done by replacing a carboxylate arm by a phosphonate/phosphinate group or by introducing a CH₂- unit in the linear or macrocyclic backbone or in a pendent arm.^{23,26,30,31} As a consequence of these changes, the bound water molecule is forced to leave faster due to the steric crowding and to the negative charge added.

Also, in the attempt to find more effective contrast agents, with optimized τ_M and τ_R values, novel Gd³⁺ chelates have been characterized.^{32,33}

4.3. Determination of τ_M

The residence lifetime of water molecules in the inner coordination sphere may be determined by analyzing the temperature dependence of the longitudinal³⁴ and transverse³⁵ relaxation rates of the water ¹⁷O resonances. The reduced relaxation rates and chemical shifts ($1/T_{1r}$, $1/T_{2r}$ and ω_t) are calculated from the relaxation rates of the

paramagnetic solutions at certain concentrations and angular frequencies of a Gd^{3+} complex ($1/T_1$, $1/T_2$ and ω) and from the

relaxation rates of the acidified water reference ($1/T_{1A}$, $1/T_{2A}$ and ω_A), which can be written as the following equations:

$$\frac{1}{T_{1r}} = \frac{1}{P_M} \left[\frac{1}{T_1} - \frac{1}{T_{1A}} \right] = \frac{1}{T_{1M} + \tau_M} + \frac{1}{T_1^{os}} \cong \frac{1}{T_{1M} + \tau_M} \quad (22)$$

$$\frac{1}{T_{2r}} = \frac{1}{P_M} \left[\frac{1}{T_2} - \frac{1}{T_{2A}} \right] = \frac{1}{\tau_M} \cdot \frac{T_{2M}^{-2} + \tau_M^{-1} T_{2M}^{-1} + \Delta\omega_M^2}{(\tau_M^{-1} + T_{2M}^{-1})^2 + \Delta\omega_M^2} + \frac{1}{T_2^{os}} \cong \frac{1}{T_{2M} + \tau_M} \quad (23)$$

$$\Delta\omega_r = \frac{1}{P_M} (\omega - \omega_A) = \frac{\Delta\omega_M}{(1 + \tau_M T_{2M}^{-1})^2 + \tau_M^2 \Delta\omega_M^2} + \Delta\omega_{os} \quad (24)$$

where $1/T_{1M}$ and $1/T_{2M}$ are the relaxation rates for the bound water, $\Delta\omega_M$ is the ^{17}O NMR chemical shift difference between the bound and bulk water and P_M is the molar fraction of the bound water. The outer sphere relaxation rate contributions ($1/T_1^{os}$ and $1/T_2^{os}$) are considered to be negligible.³⁶

The temperature dependence of τ_M follows the Eyring equation (Eq. 25), where ΔS^\ddagger and ΔH^\ddagger are the activation entropy and the activation enthalpy, respectively, for the dynamic process and k_{ex}^{298} is the water exchange rate at 298K, T is the absolute temperature.

$$\frac{1}{\tau_M} = k_{ex} = \frac{k_B T}{\hbar} \exp\left(\frac{\Delta S^\ddagger}{R} - \frac{\Delta H^\ddagger}{RT}\right) = \frac{k_{ex}^{298} T}{298.15} \exp\left[\frac{\Delta H^\ddagger}{R} \left(\frac{1}{298.15} - \frac{1}{T}\right)\right] \quad (25)$$

According to this equation, the temperature dependencies of $1/T_{1r}$ and $1/T_{2r}$ are dependent on which term dominates in the denominator of Eqs. 22 and 23. At high temperatures, when the system is in the 'fast exchange' regime,

$1/T_{2M}$ is the dominant term, and when the system is in 'slow exchange' τ_M is the dominant term. At high temperatures, the inner sphere contribution ($\Delta\omega_M$) to $\Delta\omega$ is given by the chemical shift of the bound water molecules,

which is determined by the hyperfine interaction between the unpaired electron of the Gd^{3+} and the ^{17}O nucleus, as is show in Eq. 26, where g_L is the Landé factor, μ_B is the Bohr magneton, γ_I is the gyromagnetic ratio of the nucleus (which is ^{17}O in this case), S is the electronic spin quantum number, A/\hbar is the $Gd-^{17}O$ hyperfine coupling constant and ω_I is the nuclear Larmor frequency:

$$\Delta\omega_M = \frac{g_L \mu_B}{\gamma_I} \cdot \frac{S(S+1)}{3k_B T} \cdot \frac{A}{\hbar} \omega_I \quad (26)$$

$$\frac{1}{T_{1M}} = \frac{1}{T_1^{dip}} + \frac{1}{T_1^q} = \frac{S(S+1)\gamma_I^2 \gamma_S^2 \hbar^2}{15 r^2} \left(6\tau_{1d} + \frac{14\tau_{2d}}{1 + \omega_S^2 \tau_{2d}^2} \right) + \frac{3\pi^2}{10} \left(\frac{2I+3}{I^2(2I-1)} \right) \chi^2 \left(1 + \frac{\eta^2}{3} \right) \cdot \tau_R \quad (28)$$

$$\frac{1}{\tau_{id}} = \frac{1}{\tau_M} + \frac{1}{T_{ie}} + \frac{1}{\tau_R} \quad (i=1,2) \quad (29)$$

where r is the mean Gd^{3+} -O distance, I is the nuclear spin, $\chi = (e^2 q_{zz} Q / \hbar)$ is the quadrupolar coupling constant, $\eta = (q_{xx} - q_{yy} / q_{zz})$ is the asymmetry parameter, eQ is the nuclear electric quadrupolar moment, eq_{ii} ($i=x,y,z$) are the principal values of the electric field gradient at the nucleus, and the other symbols maintain

When considered, the outer sphere contribution, $\Delta\omega_{os}$, to the chemical shift is assumed to possess a linear relation with $\Delta\omega_M$ by an empirical constant C_{os} (Eq. 27).

$$\Delta\omega_{os} = C_{os} \Delta\omega_M \quad (27)$$

The longitudinal ^{17}O NMR relaxation rate in the Gd^{3+} solution is governed by the dipole-dipole and quadrupolar mechanisms, and is described as:^{36,37}

the meaning given before. The factor $(1 + \eta^2/3)$ has the value 1 for pure water.

In the case of the transverse ^{17}O NMR relaxation, the scalar contribution is the most important mechanism and is given by Eqs. 30 and 31:

$$\frac{1}{T_{2M}} \cong \frac{1}{T_2^{SC}} = \frac{S(S+1)}{3} \left(\frac{A}{\hbar} \right)^2 \left(\tau_{1S} + \frac{\tau_{2S}}{1 + \omega_S^2 \tau_{2S}^2} \right) \quad (30)$$

$$\frac{1}{\tau_{iS}} = \frac{1}{\tau_M} + \frac{1}{T_{ie}} \quad (i=1,2) \quad (31)$$

The water exchange rate can be directly obtained from the ^{17}O NMR transverse relaxation rate, especially when the system is in the slow exchange regime (k_{ex} low compared with $1/T_{2M}$).

4.4. Reorientational Correlation Time (τ_R)

In the range of magnetic fields that are used in clinical MRI studies (0.5 – 2.0 T, that means 20 – 85 MHz), the reorientational correlation time (τ_R) is the determining parameter of the relaxivity of Gd^{3+} complexes with low molecular weight, as τ_R determines τ_c (Eq. 10). Several strategies to increase the reorientational correlation time of paramagnetic complexes have been used, based in the fact that the reorientational correlation time increases with the molecular volume of the complexes: (i) covalent attachment of the complex to large molecules such as proteins or polysaccharides,^{24,38} (ii) non-covalent binding of the complexes to macromolecules^{39,40} and (iii) a self-assembly of small chelates.^{41,42}

Figure 6 shows NMRD profiles as function of τ_R calculated from the SBM equations, where τ_R is lengthened (and τ_{c1} as well). For small molecules, τ_R values increase linearly with increasing molecular weight and for larger molecules τ_R is determined *via* both local and global rotations. Thus, internal rigidity plays an

important role in the optimization of τ_R as a function of molecular weight.

4.5. Determination of τ_R

For small spherical molecules τ_R can be estimated using the Debye-Stokes equations (Eq. 32).^{5,24}

$$\tau_R = \frac{4\pi\eta r_{\text{eff}}^3}{3k_B T} \quad (32)$$

where r_{eff} is the effective radius of the molecule, η is the microviscosity of the solution, k_B is the Boltzmann constant and T is the absolute temperature. Here, both r_{eff} and η are difficult to determine and an alternative approach is to use the τ_R dependence of the T_1 value of the water ^{17}O nuclei, where the relaxation of these nuclei in paramagnetic solutions is governed by dipolar (Eq. 6) and quadrupolar (Eq. 33) mechanisms³⁷, where I is the nuclear spin, χ is the quadrupolar coupling constant, η is the asymmetry parameter and ω_l is the nuclear Larmor frequency.

Other techniques that can be used to determine τ_R are based on ^2H and ^{13}C NMR of diamagnetic analogues of the investigated Gd^{3+} complexes.

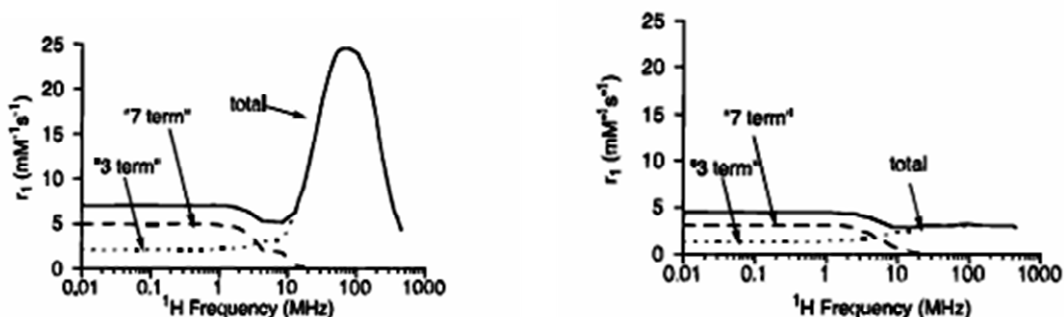


Figure 6. Simulated inner sphere relaxivities. $\tau_R = 1$ ns (left) and $\tau_R = 0.1$ ns.⁵

In the first procedure, a chemical modification is required by introducing deuterium atoms into the ligand molecule,⁴³ which is not always possible. ^2H longitudinal^{29,44} and transverse⁴⁵

relaxation rates, which are dominated by quadrupolar interactions, are measured and τ_R can be determined using Eqs. 33 and 34.

$$\frac{1}{T_1^q} = \frac{3\pi^2}{10} \left(\frac{2I+3}{I^2(2I-1)} \right) \chi^2 \cdot (1 + \eta^2/3) \left[\frac{0.2\tau_R}{1 + \omega_I^2 \tau_R^2} + \frac{0.8\tau_R}{1 + 4\omega_I^2 \tau_R^2} \right] \quad (33)$$

$$\frac{1}{T_2} (^2\text{H}) = \frac{3}{400} \left(\frac{2I+3}{I^2(2I-1)} \right) \left(1 + \frac{\eta^2}{3} \right) \chi^2 \left[3\tau_R + \frac{5\tau_R}{1 + \omega_I^2 \tau_R^2} + \frac{2\tau_R}{1 + 4\omega_I^2 \tau_R^2} \right] \quad (34)$$

When the ^{13}C NMR technique is used to determine τ_R , the dipole-dipole relaxation rate of a ^{13}C nucleus in a diamagnetic complex is measured.²⁹ This is given by Eq. 35:

$$\frac{1}{T_1^{dip}} = N \left(\frac{\mu_o}{4\pi} \right)^2 \cdot \frac{\hbar^2 \gamma_H^2 \gamma_C^2}{r_{CH}^6} \cdot \tau_R \quad (35)$$

where, \hbar is the Dirac constant, N is the number of hydrogen atoms bound to the ^{31}C nucleus and r_{CH} is the distance between the ^{31}C nucleus and a directly bound hydrogen atom. The dipole-dipole contribution to the observed relaxation rate can be determined using the

nuclear Overhauser enhancement of the corresponding resonance.

In the two latter methods, the measured relaxation rates are directly proportional to ρ_R and no separation of different contributions is needed. However, this advantage is offset by the disadvantages that a diamagnetic ion is used instead of Gd^{3+} and also that they measure the rotation of the C-H/D vector and not the rotation of the metal-coordinated water molecule.

4.6. Nuclear Magnetic Resonance Dispersion (NMRD)

The solvent water proton relaxation rate R_1 ($1/T_1$) possesses magnetic field dependence, resulting from its inner and outer sphere mechanisms. Thus, the parameters involved in the paramagnetic relaxation can be obtained through a magnetic field dependence study. This is performed by measuring the solvent proton longitudinal relaxation rates over a range of magnetic fields with a field-cycling spectrometer that switches the magnetic field strength over a range corresponding to proton Larmor frequencies. The data points represent the so-called Nuclear Magnetic Resonance Dispersion (NMRD) profile that may be fitted with Eqs. 3-11, Eqs. 14-15 and Eqs. 18-20 to obtain the values of the relaxation parameters.

Since the number of parameters involved in the relaxation process is quite high, the NMRD fittings are often subject to errors. For this reason, a accurate interpretation of

NMRD profiles can only be done by inclusion of independent information obtained from other techniques, such as: ^{17}O NMR measured at variable temperature, pressure and magnetic field for determination of τ_M , τ_R and longitudinal electronic relaxation rates;^{36,46} 2H or ^{13}C NMR also for τ_R determination;⁴³⁻⁴⁵ EPR is another very useful technique commonly used, where the line widths give direct access to transverse electronic relaxation rate.^{1,215,22}

From a NMRD profile, despite these inaccuracies, it is possible to reach some conclusions concerning the relaxation processes. First, at the high magnetic field region (10-100 MHz) the inner-sphere relaxation is governed by the reorientational correlation τ_R time, which is dependent on the molecular weight of the complexes. The NMRD profile at the low magnetic field region is mainly determined by the zero-field electronic relaxation time τ_{s0} (where $\tau_{s0}=(12\Delta^2\tau_V)^{-1}$). Thus, it depends on the symmetry of the complex and on the chemical nature of the coordinating groups. Figure 7 shows the NMRD profiles of three clinically approved CAs.⁵ All of them have one inner sphere water molecule and similar size, meaning that they have very similar τ_R values and therefore the relaxivities are almost identical at high magnetic field. However, in the low field region, the profile of the more symmetrical DOTA complex has a much higher relaxivity than the others as a consequence of its much longer zero-field electronic relaxation time τ_{s0} . The determined

τ_{S0} values are 650ps for $[\text{Gd}(\text{DOTA})(\text{H}_2\text{O})]^{-47}$ and 72 and 81ps for $[\text{Gd}(\text{DTPA})(\text{H}_2\text{O})]^{2-}$ and $[\text{Gd}(\text{DTPA-BMA})(\text{H}_2\text{O})]$, respectively.²²

5. Classes of Contrast Agents

A very high spatial resolution and the ability in distinguish soft tissues are the main advantages of MRI. However, insufficient contrast is one of the drawbacks of this technique. For this reason, a number of such substances have been developed and

researchers are directed to find more selective contrast media that would allow a better delineation of diseases thus helping radiologists in giving a more precise diagnosis. Below, are described the more recent classes of contrast agents and some examples are given providing an overview of new ideas and their applications. The conventional extracellular CAs and the hepatobiliary agents will not be discussed here, as they have been extensively discussed previously.^{5,24,48}

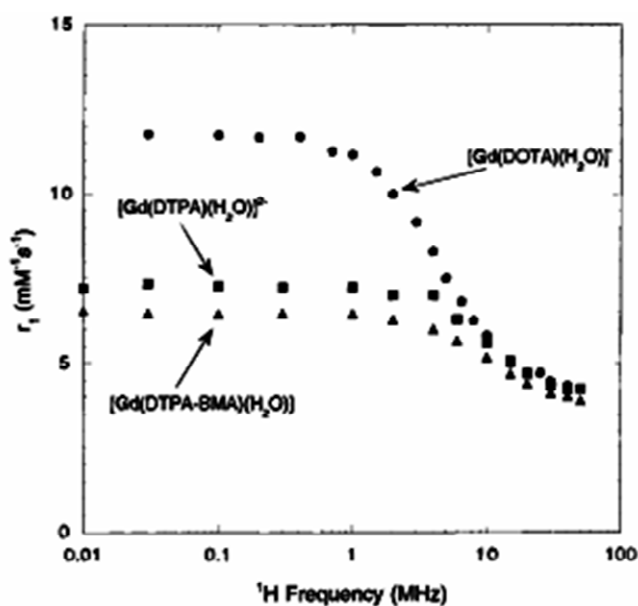


Figure 7. NMRD curves for three clinically approved Gd^{3+} chelates at 25°C.⁵

5.1. Blood Pool Agents

Blood pool agents (intravascular contrast agents) are macromolecular agents of high

molecular weight (> 20 KDa) which remain in the intravascular system for a prolonged time compared with conventional contrast agents, which diffuse quickly into the interstitial space.

Their concentration in the plasma remains stable over one hour, as its mainly renal elimination requires the previous degradation of the macromolecule. This allows imaging of the vasculature, known as magnetic resonance angiography (MRA) or cardiovascular imaging.⁵ This advantage over conventional MRI contrast media allows high resolution MRA of several organs using respiratory or cardiac gating techniques with a single contrast bolus. Vascular abnormalities, associated with certain tumors or atherosclerosis, can be detected.⁴⁸ The blood pool contrast agents can be divided in several classes: (i) small complexes interacting with

plasma proteins, (ii) system based on liposomes and (iii) systems based on polymers or particulates.⁴⁸

The most promising approach is the non-covalent binding of low molecular weight complexes to plasma proteins, in particular albumin (0.67 mM or 4.5 % concentration in the blood plasma). In this field, several complexes have been synthesized by attaching a hydrophobic moiety to a chelating agent. The most successful is the MS-325 Gd³⁺ complex (Fig. 8, right) that binds strongly and reversibly to Human Serum Albumin (HSA) in plasma⁴⁹ and which is now commercialized by Schering as Vasovist[®].

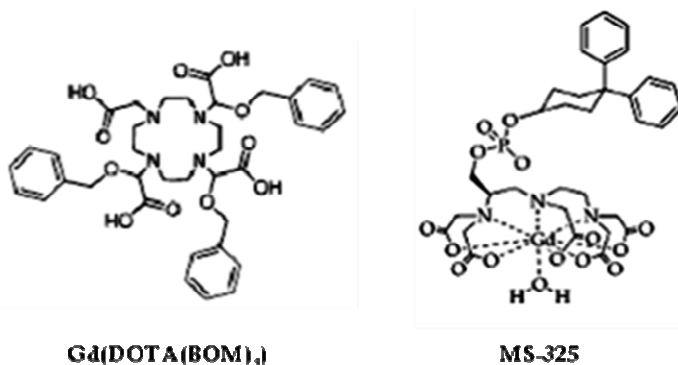


Figure 8. Structure some amphiphilic complexes able to bind plasma proteins contrast agents for MRA.

The loading of liposomes and micelles with amphiphilic polychelate polymers was reported and different paramagnetic agents have been encapsulated into the liposomes.⁵⁰⁻⁵³ Other systems that can be used as blood pool agents are polymeric or particulate compounds.

Examples of these are low molecular weight Gd³⁺ complexes conjugated to different polymers,³⁸ ultrasmall particles of iron oxides (USPIO)⁵⁴ and Gd³⁺ zeolites.⁵⁵ However, apart from the USPIOs, none of these agents has so far found a clinical

application due to high production costs and safety problems.⁵⁶

5.2. Targeting Contrast Agents

Targeting of contrast agents at a specific site (eg. a receptor) at the cellular membrane is an objective to which special attention is devoted by researchers involved in the synthesis of CAs, mainly because the development of approaches able to recognize and image a specific 'signature' of a given disease (molecular imaging) makes the task of diagnosis and therapy much easier. Thus, the development of high affinity ligands and their conjugation to contrast agents is one of the requirements for efficient molecular probes. However, the main problem of this approach using Gd³⁺ based contrast agents is that MRI is a technique of low sensitivity, so that to reach 50% of contrast enhancement it is necessary to have a local concentration of CA of the order of 0.5 mM. This, combined with the very low concentration of receptors in the cell membrane (10^{-9} - 10^{-13} mol/g of tissue) makes it difficult to obtain an image with good contrast. Also the saturation of all available receptors would interfere with the normal metabolic equilibrium, leading possibly to cell death.⁵⁷ The minimum detectable concentration of a CA depends on its relaxivity. While for [Gd(HPDO3A)] ($r_1 = 3.7 \text{ s}^{-1}\text{mM}^{-1}$ at 90 MHz) this value is too high (5×10^{-7} mol/g or 100 μM), for a 6th generation dendrimer conjugate substituted with 170 Gd-DTPA

chelates ($r_1 = 5800 \text{ s}^{-1}\text{mM}^{-1}$ per dendrimer) it has a manageable value (1.9×10^{-10} mol/g).⁵⁷ The high relaxivity of the later macromolecular CA results from the presence of a large number of Gd³⁺ chelates packed in a small volume, resulting in a high relaxivity per Gd³⁺ ion ($r_1 = 34.1 \text{ s}^{-1}(\text{mM Gd})^{-1}$, which is a consequence of the slow rotational dynamics of the CA, with some degree of internal rigidity.⁴⁸

An approach suggested by Aime *et al* to targeting tumor cells (some of which are known to have abnormally high negative charges on their cell surface) consists of a previous interaction of the tumor cell surface with a polypeptide formed by positively charged amino acids, such as polyarginine, that is suitable to interact with a negatively charged CA that is added later.⁵⁸

The targeting of cell surface receptors can be pursued by using labeled antibodies or low molecular weight targeting complexes. In the first approach, due to the slow diffusion of the antibodies, the most accessible targets are those present on the endothelial vessels. Sipkins *et al*⁵⁹ have described the targeting of the endothelial integrin $\alpha_v\beta_3$, a specific angiogenesis marker whose concentration correlates with the tumor grade. A Gd-containing polymerized liposome was used as imaging probe. Figure 9 shows the schematic representation of the process (pre-targeting approach), where firstly the target is bound to a biotinylated monoclonal antibody against $\alpha_v\beta_3$, which is well recognized by an avidin

moiety present on the liposome surface, which carries the Gd^{3+} chelate reporter groups.

Recently, the same $\alpha_v\beta_3$ target has been addressed with lipidic nanoparticles containing Gd^{3+} chelates.⁶⁰ Although the possibility of extensive substitution of some antibodies without loss of immunoreactivity, has been

demonstrated when they are labeled with liposomes, dendrimers or polymeric chelates and nanoparticles, the large molecular size of these systems limits the technique.⁴⁸ For this reason, the search for low molecular weight targeting CAs able to accumulate quickly at specific cell surface sites was stimulated.

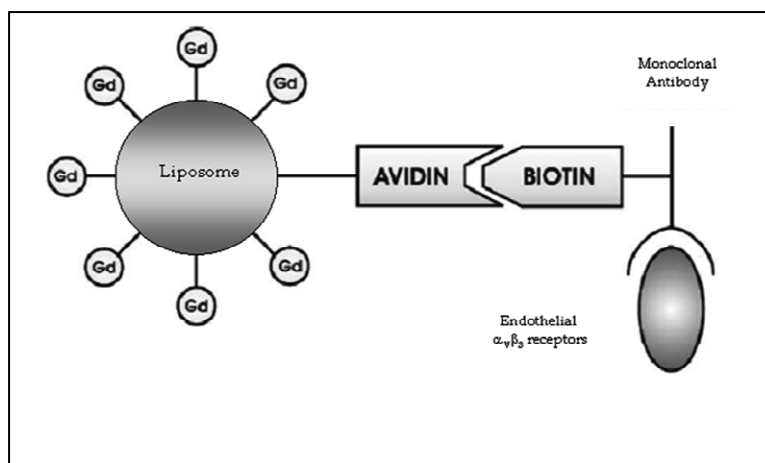


Figure 9. Schematic representation of targeting of the endothelial $\alpha_v\beta_3$ angiogenesis marker.⁵⁹

Frullano *et al* have reported a study in the field of low molecular weight targeting CAs that is based on the abnormal glycosilation of tumor cell surfaces, which have much higher content of sialic acid residues ($> 10^9$ /cell) than normal cells ($\sim 10^6$ /cell), where the sialic acid residues are recognized by a modified Gd^{3+} chelate.⁶¹

Another way to accumulate CAs at the target site is by cell internalization processes, in which for a successful internalization process, the concentration of the agent inside the cell

should be higher than at the cell surface. These internalization processes may occur via receptor mediated endocytosis or via pinocytosis and phagocytosis mechanisms. Concerning cell internalization via receptors, an interesting example is the entrapment of several units of CA inside the inner spherical cavity of apoferritin (Fig. 10), which after intravenous administration is quickly cleared-up by specific receptors on hepatocytes.^{62,63} Among a number of systems, Gd-HPDO3A is a good candidate to labeling stem cells via the

pinocytosis mechanism,⁶⁴ where a few millions of stem cells are incubated in a culture medium containing GdHPDO3A in the mM concentration range (10-50 mM). Another internalization mechanism that can be exploited is by phagocytosis, the process of internalization of particles by cells endowed with phagocytic activity. This goal was reached by Aime *et al*, where the phagocytosis occurs with Gd^{3+} -DTPA bis-stearylamine derivatives forming biodegradable Gd-containing particles. These were designed so that the insolubility is a property of the Gd^{3+} chelates themselves.⁶⁵

5.3. Responsive Contrast Agents

The term 'responsive' refers to paramagnetic systems that are sensitive to a given physico-chemical parameter that

characterizes their microenvironment. Typical parameters to which these systems should be responsive are (i) pH, (ii) temperature, (iii) oxygen pressure, (iv) enzymatic activity, (v) redox potential and (vi) concentration of a specific ion.

pH sensitive

These CAs are of great interest in cancer detection, as the pH at the surface of tumors is about 0.4 units lower than for normal tissue. The requirement for a system to be pH-sensitive is that either the dynamics or structural properties determining its relaxivity are pH-dependent. The pH dependence of the relaxivity reflects changes in the hydration number of the metal chelates and the presence of protonatable groups on the ligands can influence these changes.⁶⁶

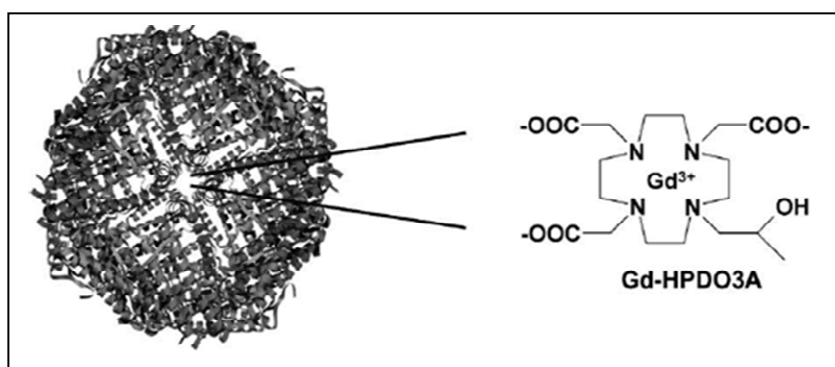


Figure 10. Schematic representation of Gd-HPDO3A loaded apoferritin.⁶²

In a Gd^{3+} complex bearing an arylsulfonamide group, it has been demonstrated that the observed decrease in the relaxivity with

increasing pH is due to the presence of two water molecules in the inner sphere of the complex at acid pH, while at high pH no

coordinated water is present (Fig. 11). In another case, Zhang *et al* have demonstrated that the pH dependence of the relaxivity of GdDOTA-4AmP (amino phosphonate tetraamide derivative) is due to changes in the

second coordination sphere,⁶⁸ where these changes are related with the formation/disruption of hydrogen bonds between the pendant phosphonate groups and water molecules bound to the Gd^{3+} ion.

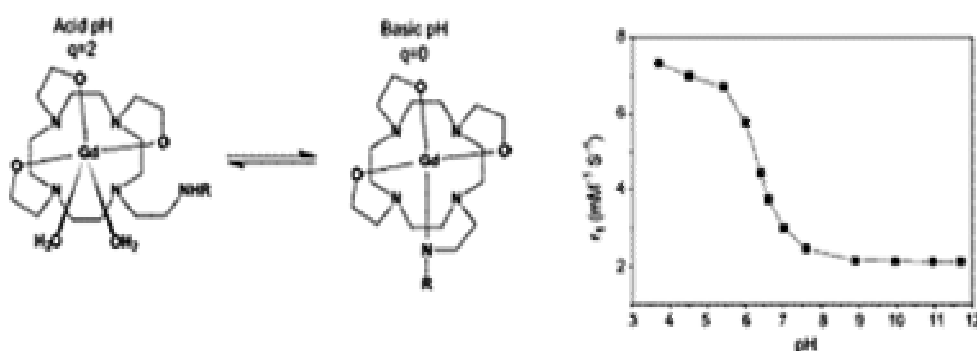


Figure 11. pH dependence of the relaxivity of a Gd^{3+} complex bearing a arylsulfonamide group (20MHz, 25°C).⁶⁷

An example of how the changes in dynamic properties affect the relaxivity is represented by a polyamino acid conjugated with Gd^{3+} complexes (Fig. 12).⁶⁹ In this case, depending on the protonation state of the free amino groups, the tertiary structure of the polymer is random and flexible (at low pH) when they are protonated, as they tend to stay as far from each other as possible giving a low relaxivity, or can adopt a more rigid and compact structure with higher relaxivity (at high pH) due to the formation of intramolecular hydrogen bonds between adjacent peptidic linkage (Fig. 12).

Recently Tóth *et al*, have reported a Gd-fullerene water soluble in which the relaxivity is

pH dependent, which is a good candidate for applications in this field.⁷⁰

Temperature sensitive

It is known that some Ln^{3+} chelates have temperature dependent NMR properties and their 1H NMR chemical shifts are applied for their monitoring. For this reason, some of them are considered to be good temperature probes.^{71,72}

Another example of a temperature dependent probe consists of the encapsulation of Gd^{3+} chelates into liposomes.⁷³ Here, the membrane transition from gel to liquid crystal occurs at a certain temperature. At this point, changes in the permeability of the membrane occur and the mobility of the water molecules

through the membrane changes, consequently the relaxivity also changes.

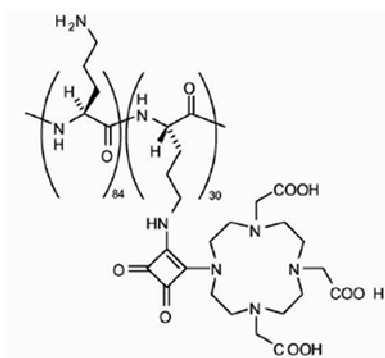


Figure 12. Chemical structure of the macromolecular construct formed by 30 Gd^{3+} units covalently linked by a squaric acid moiety to a poly-ornithine.⁶⁹

Agents sensitive to the redox potential

The partial oxygen pressure (pO_2) is also an important parameter in the metabolic processes of the cells and its variation is related with certain pathologies. The usual systems used as pO_2 probes are based on the redox equilibria of paramagnetic ions, such as Mn^{2+}/Mn^{3+} and Eu^{2+}/Eu^{3+} . The relaxivity of these systems depends on the oxidation state of the metal ion and thus is dependent on the oxygen pressure.⁷⁴

CAs sensitive to enzyme activity

The strategy used by Anelli *et al* to obtain enzyme responsive agents was to synthesize a linear Gd^{3+} complex possessing an arylsulfonamide moiety that is an inhibitor of carbonic anhydrase (Fig.13).⁷⁵ Here, the relaxivity is enhanced as a result of the

increased reorientational correlation time τ_R upon interaction with the enzyme.

The alternative approach used is the development of Gd^{3+} complexes acting as a substrate for a specific enzyme. The strategy now is that the enzyme specific contrast agents are converted by specific enzymes into compounds with higher relaxivity. Some examples are: (i) a Gd^{3+} -DTPA derivative with a negatively charged phosphorylated side-chain, which does not interact with HSA, is responsive to alkaline phosphatase activity, as hydrolysis of this side-chain yields an hydrophobic moiety well suited to bind to HSA and increase r_1 .⁷⁶ (ii) A Gd -DO3A derivative responsive to β -galactosidase activity.⁷⁷

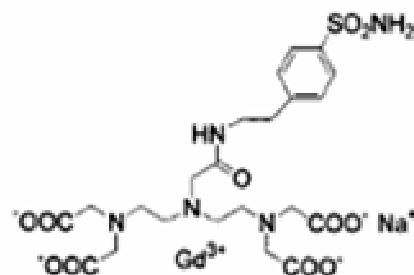


Figure 13. Chemical structure of a Gd^{3+} complex which shows a high binding affinity towards carbonic anhydrase.⁷⁵

Metal ion and radical responsive CAs

Here, the presence of metal ions can induce changes in the structure of the paramagnetic complexes, changing consequently their relaxivities. Calcium and iron responsive systems have been reported.^{78,79} In the first case, two Gd^{3+} complexes are conjugated via a Ca^{2+} binding spacer. In the presence of calcium its

coordination occurs by shifting of four carboxylate groups (two for each Gd^{3+} chelate) from the Gd^{3+} to the Ca^{2+} ion. Consequently two water molecules will coordinate in the inner sphere of the complexes, giving an increase in the relaxivity (Fig. 14).⁷⁸

Recently, a novel radical responsive CA has been reported, which consists of Gd^{3+} chelates conjugated to a liposome through a disulfide linker (Fig. 15). The disulfide bonds represent a radical-sensitive moiety and a large decrease in the relaxivity is observed upon their cleavage.⁸⁰

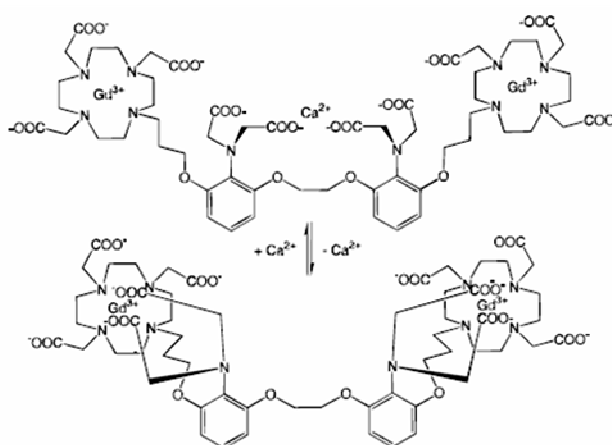


Figure 14. Schematic representation of $Gd(DOPTA)$ displaying different conformations in the presence of Ca^{2+} ions.⁷⁸

5.4. Chemical Exchange Saturation Transfer (CEST) Agents

Some years ago, a new class of contrast agents that is based on the chemical exchange saturation transfer has been proposed.⁸¹ Basically a CEST agent is a molecule containing mobile protons, whose exchange rate with the bulk water protons is slow in the NMR timescale. In other words, the exchange rates between the mobile protons and the bulk water molecules must be smaller than the

difference in frequency ($\Delta\omega$) between the respective chemical environments, $\Delta\omega \geq k_{ex}$. When this condition is fulfilled, the resonance of the mobile protons of the CEST agent may be selectively saturated by using a specific radio frequency B_1 and then the chemical exchange process transfers the saturated magnetization from the mobile protons of the CEST agent to the bulk water molecules, whose signal intensity will decrease accordingly (Fig. 16).

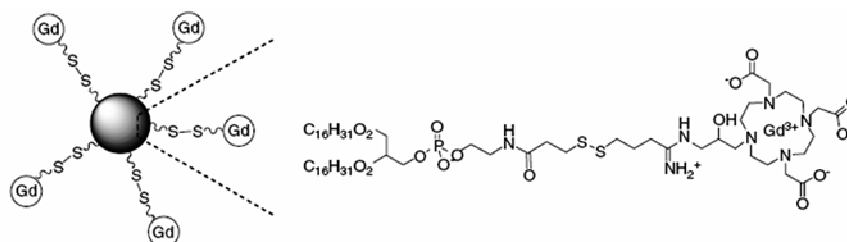


Figure 15. Schematic representation of Gd-HASH-DO3A conjugated to liposome.⁸⁰

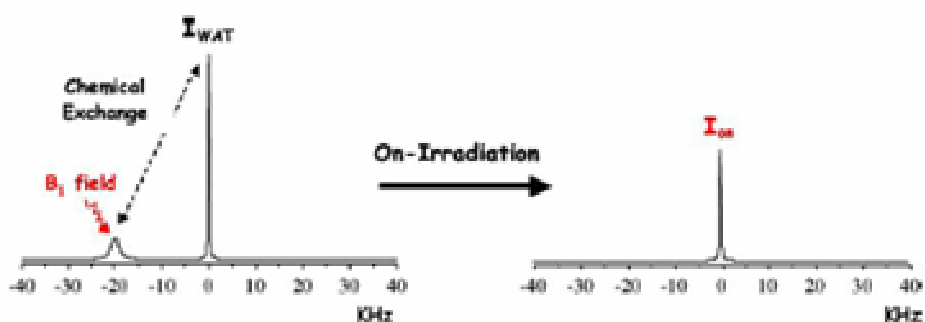


Figure 16. Scheme of a CEST process.⁶⁷

Since $\Delta\omega$ increases with the magnetic field strength, the overall relationship between $\Delta\omega$ and k_{ex} will be a function of the field strength of the MR experiment. A larger $\Delta\omega$ value improves the specificity of the CEST effect because for many tissues the magnetic field inhomogeneity, which will broaden their resonances, can exceed 2ppm.⁸²

Since the attainable saturation transfer (ST) value is directly related to k_{ex} , it is expected that paramagnetic complexes, displaying large $\Delta\omega$ values for the exchanging proton

resonance, may improve the efficacy of the CEST agents. These so called PARACEST agents consist of particular Ln^{3+} complexes with a coordinated water molecule undergoing extremely slow exchange with the bulk water, and with very large $\Delta\omega$ values. Zhang *et al* reported a good ST effect by irradiating the metal-bound water protons of Eu^{3+} chelates resonating at 50 ppm downfield from the bulk water.⁸³ The same effect can be obtained with slow exchanging amide protons of Ln^{3+} complexes of DOTA derivatives.⁸⁴ Recently, it

has been reported that paramagnetic Ln^{3+} complexes of tetraamide derivatives of DOTA (Fig. 17) show ST properties which are markedly dependent on pH and lactate concentration, making them responsive CAs.⁸⁵⁻⁸⁷

An advantage of CEST agents relative to the traditional MRI CAs is that the generation of contrast occurs only if the rf irradiation frequency to the absorption frequency is set equal of the mobile protons. For this reason, the registration of an image before the CEST agent administration is not required because the image visualization of CEST agents results from the comparison of the on and off resonance MRI scan. Furthermore, a co-administration of different CEST agents at same time is possible (since the difference on

resonance frequencies of their mobile protons is large enough to avoid the overlapping of the respective CEST resonances) making possible the detection of their biodistribution in the same image.⁸⁸ In this way, it is possible to make the CEST response independent of the absolute concentration of the agent by using ratiometric methods.

The most critical disadvantage of CEST agents is their low sensitivity. Theoretically, the ST process is dependent on a lot of parameters, among which k_{ex} and the number of mobile protons available are particularly relevant. Small sized CEST agents, containing less than 10 mobile protons per molecule, such as amino acids, heterocyclic compounds, sugars or paramagnetic chelates, have the detection limit in the range of mM.^{81,86,87,89}

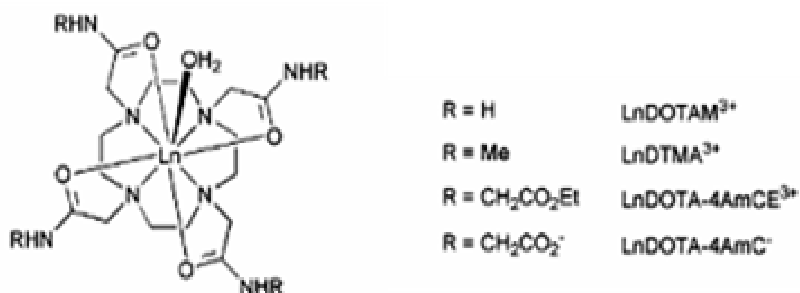


Figure 17. Structure of some DOTA tetra-amides studied as CEST CAs.

To solve this problem, some approaches were suggested in order to increase the number of mobile protons in the CEST agents, among which the investigation of the ST properties in macromolecules, both

diamagnetic (polyaminoacids, dendrimers and RNA-like polymers) and paramagnetic ones,⁹⁰⁻⁹² in which their detection limit goes down into the range of μM . Another approach to improve the sensitivity of CEST agents is represented

by liposomes, which are water-permeable lipidic vesicles commonly used in the pharmaceutical field as drug delivery systems. Here the number of mobile protons which can be entrapped in a liposome cavity is in the range of 10^6 - 10^9 , depending on the liposome size. Besides the water molecules, an efficient paramagnetic shift reagent, such as

[Tm(DOTMA)], is also entrapped in the liposome cavity, shifting the proton resonance of trapped water relative to the bulk water. Due to the slow water exchange across the liposome membrane, this type of assembly (Fig. 18), named LIPOCEST agent, can be used to generate a CEST image at nM concentration.⁹³

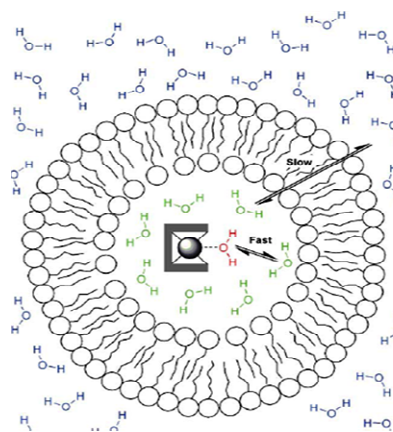
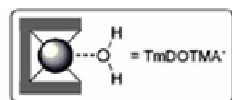


Figure 18. Schematic representation of the encapsulation of water molecules and a paramagnetic complex into the liposome cavity to be used as PARACEST agent.

6. Conclusions

The clinical success of the commercialized non-specific, hepatobiliary and angiographic Gd³⁺-based MRI contrast agents is quite clear. However, the development of clinically acceptable targeted and responsive CAs is a much greater challenge. One obvious task for the design of these new generation agents is to improve the proton relaxivity of their reporter groups. Slowing down the rotation of these

agents by conjugation to macromolecules has led to much lower relaxivity gains than expected on the basis of the increase of molecular weight, mainly due to lack of rigidity of the linker, but also to the difficulty of simultaneously optimizing the rotational, water exchange and electron spin relaxation parameters. A proper ligand design still may overcome this problem.⁹⁴

Another major challenge for MRI-based targeted CAs being usable as molecular

imaging agents is the efficient delivery of a high payload (tens, hundreds or even thousands) of reporter groups to each target site. In fact, an ideal targeted MRI CA should allow the detection of molecular events at the nM concentration range. For this purpose, LIPOCEST agents and nanoparticulate CAs seem to be the most promising approaches.⁹⁵

Acknowledgments

This work was supported by the Foundation of Science and Technology (FCT), Portugal (project POCTI/QUI/47005/2002 Ph.D. grant SFRH/BD/9685/2002 to GAP) and FEDER. It was carried out in the frame of the EC COST Action D38 "Metal-Based Systems for Molecular Imaging Applications" and the EU Network of Excellence European Molecular Imaging Laboratory" (EMIL, LSCH-2004-503569).

References

- Damadian, R. *Science* **171** (1971) 1151.
- (a) Lauterbur, P. C. *Nature* **242** (1973) 190 ; (b) Mansfield, P.; Grannell, P.K. *J. Phys. C: Solid State Physics*. **6** (1973) L422.
- Hornak, J. P. Basics of MRI. A Hyperbook on magnetic resonance imaging (Copyright (C)1996-003). www.cis.rit.edu/htbooks/mri.
- Brown, M. A.; Semelka, R. L. *MRI - Basic Principles and Applications*, Wiley-Liss, Hoboken, New Jersey, 2003.
- Caravan, P.; Ellison, J. J.; McMurry, T. J.; Lauffer, R. B. *Chem.Rev.* **99** (1999) 2293.
- Toth, E.; Helm, L.; Merbach, A. E. *Top.Curr.Chem.* **61** (2002) 221.
- Botta, M. *Eur.J.Inorg.Chem.* **2000** (2000) 399.
- Solomon, I. *Phys.Rev.* **99** (1955) 559.
- Bloembergen N.; Morgan L.O. *J.Chem.Phys.* **34** (1961) 842.
- Bloembergen, N. *J.Chem.Phys.* **27** (1957) 572.
- Peters, J. A.; Huskens, J.; Raber, D. J. *Prog.Nuc.Magn.Reson.Spect.* **28** (1996) 283.
- Gueron, M. *J.Magn.Reson.* **19** (1975) 58.
- McLachlan, A. D. *Proc.R.Soc.London A* **280** (1964) 271..
- Bertini, I.; Luchinat, C. *Coord.Chem.Rev.* **150** (1996) 1.
- Powell, D. H.; Merbach, A. E.; Gonzalez, G.; Brücker, E.; Micskei, K.; Ottaviani, M. F.; Köhler, K.; Zelewsky, A. V.; Grinberg, O. Y.; Lebedev, Y. S. *Helv.Chim.Acta* **76** (1993) 2129.
- Rast, S.; Borel, A.; Helm, L.; Belorizky, E.; Fries, P. H.; Merbach, A. E. *J.Am.Chem.Soc.* **123** (2001) 2637.
- Freed, J. H. *J.Chem.Phys.* **68** (1978) 4034.
- Koenig, S. H.; Brown III, R. D. *Prog. Nuc. Magn. Reson. Spect.* **22** (1991) 487.
- Avecilla, F.; Peters, J. A.; Geraldes, C. F. G. C. *Eur.J.Inorg.Chem.* **2003** (2003) 4179.
- Hajela, S.; Botta, M.; Giraudo, S.; Xu, J.; Raymond, K. N.; Aime, S. *J.Am.Chem.Soc.* **122** (2000) 11228.

21. Aime, S.; Botta, M.; Frullano, L.; Crich, S. G.; Giovenzana, G.; Pagliarin, R.; Palmisano, G.; Sirtori, F. R.; Sisti, M. *J.Med.Chem.* **43** (2000) 4017.
22. Powell, D. H.; Dhubhghaill, O. M. N.; Pubanz, D.; Helm, L.; Lebedev, Y. S.; Schlaepfer, W.; Merbach, A. E. *J.Am.Chem.Soc.* **118** (1996) 9333.
23. Rudovský, J.; Hermann, P.; Botta, M.; Aime, S.; Lukes, I. *Chem.Commun.* **2005** (2005) 2390.
24. Lauffer, R. B. *Chem.Rev.* **87** (1987) 901.
25. Aime, S.; Barge, A.; Bruce, J. I.; Botta, M.; Howard, J. A. K.; Moloney, J. M.; Parker, D.; de Sousa, A. S.; Woods, M. *J Am Chem Soc* **121** (1999) 5762.
26. Kotek, J.; Lebduskova, P.; Hermann, P.; Vander Elst, L.; Muller, R. N.; Geraldès, C. F.; Maschmeyer, T.; Lukes, I.; Peters, J. A. *Chem.Eur.J.* **9** (2003) 5899.
27. Pubanz, D.; Gonzalez, G.; Powell, D. H.; Merbach, A. E. *Inorg.Chem.* **34** (1995) 4447.
28. Toth, É.; Burai, L.; Brücker, E.; Merbach, A. E. *J.Chem.Soc., Dalton Trans.* **1997** (1997) 1587.
29. Lammers, H.; Maton, F.; Pubanz, D.; van Laren, M. W.; van Bekkum, H.; Merbach, A. E.; Muller, R. N.; Peters, J. A. *Inorg.Chem.* **36** (1997) 2527.
30. Ruloff, R.; Toth, E.; Scopelliti, R.; Tripier, R.; Handel, H.; Merbach, A. E. *Chem Commun (Camb)* (2002) 2630.
31. Laus, S.; Ruloff, R.; Toth, E.; Merbach, A. E. *Chem.Eur.J.* **9** (2003) 3555.
32. Aime, S.; Calabi, L.; Cavallotti, C.; Gianolio, E.; Giovenzana, G. B.; Losi, P.; Maiocchi, A.; Palmisano, G.; Sisti, M. *Inorg.Chem.* **43** (2004) 7588.
33. Livramento, J. B.; Toth, E.; Sour, A.; Borel, A.; Merbach, A. E.; Ruloff, R. *Angew.Chem.Int.Ed.Engl.* **44** (2005) 1480.
34. Zimmerman, J. R.; Brittin, W. E. *J.Phys.Chem.* **61** (1957) 1328.
35. Swift, T. J.; Connick, R. E. *J.Chem.Phys.* **37** (1962) 307.
36. Micskei, K.; Helm, L.; Brucher, E.; Merbach, A. E. *Inorg.Chem.* **32** (1993) 3844.
37. Micskei, K.; Powell, D. H.; Helm, L.; Brücker, E.; Merbach, A. E. *Magn.Reson.Chem.* **31** (1993) 1011.
38. Corsi, D. M.; Elst, L. V.; Muller, R. N.; van Bekkum, H.; Peters, J. A. *Chem.Eur.J.* **7** (2001) 64.
39. Caravan, P.; Cloutier, N. J.; Greenfield, M. T.; McDermid, S. A.; Dunham, S. U.; Bulte, J. W. M.; Amedio, J. C.; Looby, R. J.; Supkowski, R. M.; Horrocks, W. D.; McMurry, T. J.; Lauffer, R. B. *J.Am.Chem.Soc.* **124** (2002) 3152.
40. Aime, S.; Mauro, B.; Mauro, F.; Simonetta, G. C.; Enzo, T. *J.Biol.Inorg.Chem.* **1** (1996) 312.
41. André, J. P.; Tóth, E.; Fischer, H.; Seelig, A.; Mäcke, H. R.; Merbach, A. E. *Chem.Eur.J.* **5** (1999) 2977.
42. Accardo, A.; Tesauro, D.; Roscigno, P.; Gianolio, E.; Paduano, L.; D'Errico, G.; Pedone, C.; Morelli, G. *J.Am.Chem.Soc.* **126** (2004) 3097.
43. Wheeler, W. D.; Legg, J. I. *Inorg.Chem.* **24** (1985) 1292.
44. Iglesias, C. P.; Corsi, D. M.; Elst, L. V.; Muller, R. N.; Imbert, D.; Bünzli, J. C. G.; Toth, E.; Maschmeyer, T.; Peters, J. A. *J.Chem.Soc., Dalton Trans.* **2003** (2003) 727.
45. Elst, L. V.; Port, M.; Raynal, I.; Simonot, C.; Muller, R. N. *Eur.J.Inorg.Chem.* **2003** (2003) 2495.

46. Gonzalez, G.; Powell, D. H.; Tissieres, V.; Merbach, A. E. *J.Phys.Chem.* **98** (1994) 53.
47. Geraldes, C. F. G. C.; Sherry, A. D.; Lazar, I.; Miseta, A.; Bogner, P.; Berenyi, E.; Sumegi, B.; Kiefer, G. E.; McMillan, K.; Maton, F. *Magn.Reson.Chem.* **30** (1993) 696.
48. Jacques, V.; Desreux, J. F. *Top.Curr.Chem.* **221** (2002) 123.
49. Lauffer, R. B.; Parmelee, D. J.; Dunham, S. U.; Ouellet, H. S.; Dolan, R. P.; Witte, S.; McMurry, T. J.; Walovitch, R. C. *Radiology* **207** (1998) 529.
50. Torchilin, V. P. *Curr.Pharm.Biotechnol.* **1** (2000) 183.
51. Lokling, K. E.; Skurtveit, R.; Fossheim, S. L.; Smistad, G.; Henriksen, I.; Klaveness, J. *Magn.Reson.Chem.* **21** (2003) 531.
52. Gløgård, C.; Stensrud, G.; Hovland, R.; Fossheim, S. L.; Klaveness, J. *Int.J.Pharm.* **233** (2002) 131.
53. Lokling, K. E.; Fossheim, S. L.; Skurtveit, R.; Bjornerud, A.; Klaveness, J. *Magn Reson Imaging* **19** (2001) 731.
54. Weissleder, R.; Elizondo, G.; Wittenberg, J.; Rabito, C. A.; Bengel, H. H.; Josephson, L. *Radiology* **175** (1990) 489.
55. Iglesias, C. P.; Elst, L. V.; Zhou, W.; Muller, R. N.; Geraldes, C. F. G. C.; Maschmeyer, T.; Peters, J. A. *Chem.Eur.J.* **8** (2002) 5121.
56. Bogdanov, A. A.; Lewin, M.; Weissleder, R. *Adv.Drug.Deliv.Rev.* **37** (1999) 279.
57. Nunn, A. D.; Linder, K. E.; Tweedle, M. F. *Q.J.Nucl.Med.* **41** (1997) 155.
58. Aime, S.; Botta, M.; Garino, E.; Crich, S. G.; Giovenzana, G.; Pagliarin, R.; Palmisano, G.; Sisti, M. *Chem.Eur.J.* **6** (2000) 2609.
59. Sipkins, D. A.; Cheresch, D. A.; Kazemi, M. R.; Nevin, L. M.; Bednarski, M. D.; Li, K. C. *Nat Med* **4** (1998) 623.
60. Winter, P. M.; Caruthers, S. D.; Kassner, A.; Harris, T. D.; Chinen, L. K.; Allen, J. S.; Lacy, E. K.; Zhang, H.; Robertson, J. D.; Wickline, S. A.; Lanza, G. M. *Cancer Res.* **63** (2003) 5838.
61. Frullano, L.; Rohovec, J.; Aime, S.; Maschmeyer, T.; Prata, M. I.; de Lima, J. J.; Geraldes, C. F. G. C.; Peters, J. A. *Chem.Eur.J.* **10** (2004) 5205.
62. Aime, S.; Frullano, L.; Crich, S. G. *Angew.Chem.Int.Ed.Engl.* **41** (2002) 1017.
63. Osterloh, K.; Aisen, P. *Biochim.Biophys.Acta.* **1011** (1989) 40.
64. Crich, S. G.; Biancone, L.; Cantaluppi, V.; Duo, D.; Esposito, G.; Russo, S.; Camussi, G.; Aime, S. *Magn.Reson.Chem.* **51** (2004) 938.
65. Aime, S.; Cabella, C.; Colombatto, S.; Geninatti Crich, S.; Gianolio, E.; Maggioni, F. *J.Magn.Reson.Imaging* **16** (2002) 394.
66. Lowe, M. P.; Parker, D.; Reany, O.; Aime, S.; Botta, M.; Castellano, G.; Gianolio, E.; Pagliarin, R. *J.Am.Chem.Soc.* **123** (2001) 7601.
67. Aime, S.; Crich, S. G.; Gianolio, E.; Tei, L.; Terreno, E. *Coord.Chem.Rev.* **250** (2006) 1562.
68. Zhang, S.; Wu, K.; Sherry, A. D. *Angew Chem Int Ed Engl* **38** (1999) 3192.
69. Aime, S.; Crich, S. G.; Botta, M.; Giovenzana, G.; Palmisano, G.; Sisti, M. *Chem.Comm.* **1999** (1999) 1578.
70. Toth, E.; Bolskar, R. D.; Borel, A.; Gonzalez, G.; Helm, L.; Merbach, A. E.; Sitharaman, B.; Wilson, L. J. *J.Am.Chem.Soc.* **127** (2005) 799.

71. Aime, S.; Botta, M.; Fasano, M.; Terreno, E.; Kinchesh, P.; Calabi, L.; Paleari, L. *Magn.Reson.Chem.* **35** (1996) 648.
72. Zuo, C. S.; Mahmood, A.; Sherry, A. D. *J.Magn.Reson.* **151** (2001) 101.
73. Fossheim, S. L.; Il'yasov, K. A.; Hennig, J.; Bjornerud, A. *Acad.Radiol.* **7** (2000) 1107.
74. Aime, S.; Botta, M.; Gianolio, E.; Terreno, E. *Angew.Chem.Int.Ed.Engl.* **39** (2000) 747.
75. Anelli, P. L.; Bertini, I.; Fragai, M.; Lattuada, L.; Luchinat, C.; Parigi, G. *Eur.J.Inorg.Chem.* **2000** (2000) 625.
76. Lauffer, R. B., McMurry, T. J., Dunham, S. U., Scott, M. J., Parmelee, D. J., and Dumas, S. US Patent *PCT Int. Appl.*, WO9736619 (1997).
77. Moats, R. A.; Fraser, S. E.; Meade, T. J. *Angew.Chem.Int.Ed.Engl.* **36** (1997) 726.
78. Li, W. H.; Fraser, S. E.; Meade, T. J. *J.Am.Chem.Soc.* **121** (1999) 1413.
79. Comblin, V.; Gilsoul, D.; Hermann, M.; Humblet, V.; Jacques, V.; Mesbahi, M.; Sauvage, C.; Desreux, J.F. *Coord.Chem.Rev.* **185-186** (1999) 451.
80. Gløgaard C.; Stensrud G.; Aime S. *Magn.Reson.Chem.* **41** (2003) 585.
81. Ward, K. M.; Aletras, A. H.; Balaban, R. S. *J.Magn.Reson.* **143** (2000) 79.
82. Guivel-Scharen, V.; Sinnwell, T.; Wolff, S. D.; Balaban, R. S. *J.Magn.Reson.* **133** (1998) 36.
83. Zhang, S.; Winter, P.; Wu, K.; Sherry, A. D. *J.Am.Chem.Soc.* **123** (2001) 1517.
84. Zhang, S.; Merritt, M.; Woessner, D. E.; Lenkinski, R. E.; Sherry, A. D. *Acc.Chem.Res.* **36** (2003) 783.
85. Aime, S.; Castelli, D. D.; Terreno, E. *Angew.Chem.Int.Ed.Engl.* **41** (2002) 4334.
86. Aime, S.; Barge, A.; Castelli, D. D.; Fedeli, F.; Mortillaro, A.; Nielsen, F. U.; Terreno, E. *Magn.Reson.Chem.* **47** (2002) 639.
87. Zhang, S.; Michaudet, L.; Burgess, S.; Sherry, A. D. *Angew. Chem. Int. Ed. Engl.* **41** (2002) 1919.
88. Aime, S.; Carrera, C.; Castelli, D. D.; Crich, S. G.; Terreno, E. *Angew Chem Int Ed Engl* **44** (2005) 1813.
89. Terreno, E.; Castelli, D. D.; Cravotto, G.; Milone, L.; Aime, S. *Invest.Radiol.* **39** (2004) 235.
90. Goffeney, N.; Bulte, J. W.; Duyn, J.; Bryant, L. H.; van Zijl, P. C. *J.Am.Chem.Soc.* **123** (2001) 8628.
91. Snoussi, K.; Bulte, J. W.; Gueron, M.; van Zijl, P. C. *Magn.Reson.Med.* **49** (2003) 998.
92. Aime, S.; Castelli, D. D.; Terreno, E. *Angew.Chem.Int.Ed.Engl.* **42** (2003) 4527.
93. Aime, S.; Castelli, D. D.; Terreno, E. *Angew.Chem.Int.Ed.Engl.* **44** (2005) 5513.
94. Merbach, A. E.; Tóth, E. Eds. *The Chemistry of Contrast Agents in Medical Magnetic Resonance Imaging*, John Wiley and Sons (2001).
95. Muller, R. N.; Elst, L.; Roch, A.; Peters, J.A.; Csajbók, E; Gillis, P; Gossuin, Y. *Adv. Inorg. Chem.* **57** (2005) 239.